Supplement of Atmos. Meas. Tech., 16, 4445–4460, 2023
https://doi.org/10.5194/amt-16-4445-2023-supplement

Atmospheric Measurement Techniques
Open Access
EGU

Supplement of

Pressure-dependent performance of two CEN-specified condensation particle counters

Paulus S. Bauer et al.

Correspondence to: Bernadett Weinzierl (bernadett.weinzierl@univie.ac.at)

1 Derivation of heat and mass transfer equations

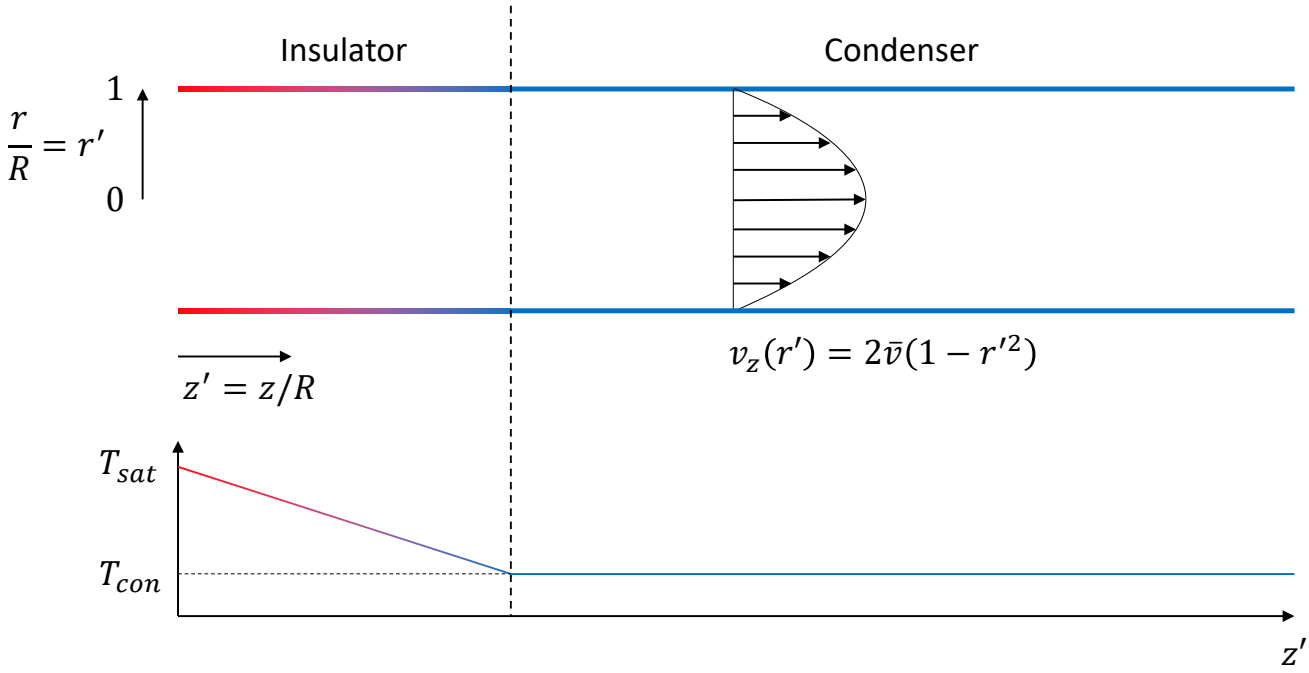

Figure S1: Sketch of the insulator and condenser tube inside a CPC for the simulation. We made several assumptions, which are listed in Sect. 2.3 Simulation Methods in the publication.

The equations of energy (Eq. (1), with temperature T) and continuity (Eq. (2) with partial vapor pressure p_v of the condensing vapor) for Newtonian fluids in cylindrical coordinates (r, Θ, z) are as follows (Bird et al., 2002):

$$\begin{aligned} \frac{\rho C}{k} \cdot \frac{dT}{dt} &= \nabla^2 T, \\ \frac{\rho C}{k} \cdot \left(\frac{\partial r}{\partial t}\frac{\partial T}{\partial r} + \frac{1}{r}\frac{\partial \Theta}{\partial t}\frac{\partial T}{\partial \Theta} + \frac{\partial z}{\partial t}\frac{\partial T}{\partial z} + \frac{\partial T}{\partial t} \right) &= \frac{1}{r}\frac{\partial}{\partial r}\left(r\frac{\partial T}{\partial r} \right) + \frac{1}{r^2}\frac{\partial^2 T}{\partial \Theta^2} + \frac{\partial^2 T}{\partial z^2}, \quad (1) \\ \frac{\rho C}{k} \cdot \left(v_r\frac{\partial T}{\partial r} + \frac{v_\Theta}{r}\frac{\partial T}{\partial \Theta} + v_z\frac{\partial T}{\partial z} + \frac{\partial T}{\partial t} \right) &= \frac{1}{r}\frac{\partial}{\partial r}\left(r\frac{\partial T}{\partial r} \right) + \frac{1}{r^2}\frac{\partial^2 T}{\partial \Theta^2} + \frac{\partial^2 T}{\partial z^2}. \end{aligned}$$

Here ρ is the density, C the heat capacity and k the conductivity of the fluid.

$$\begin{aligned} \frac{1}{D} \cdot \frac{dp_v}{dt} &= \nabla^2 p_v, \\ \frac{1}{D} \cdot \left(\frac{\partial r}{\partial t}\frac{\partial p_v}{\partial r} + \frac{1}{r}\frac{\partial \Theta}{\partial t}\frac{\partial p_v}{\partial \Theta} + \frac{\partial z}{\partial t}\frac{\partial p_v}{\partial z} + \frac{\partial p_v}{\partial t} \right) &= \frac{1}{r}\frac{\partial}{\partial r}\left(r\frac{\partial p_v}{\partial r} \right) + \frac{1}{r^2}\frac{\partial^2 p_v}{\partial \Theta^2} + \frac{\partial^2 p_v}{\partial z^2}, \quad (2) \\ \frac{1}{D} \cdot \left(v_r\frac{\partial p_v}{\partial r} + \frac{v_\Theta}{r}\frac{\partial p_v}{\partial \Theta} + v_z\frac{\partial p_v}{\partial z} + \frac{\partial p_v}{\partial t} \right) &= \frac{1}{r}\frac{\partial}{\partial r}\left(r\frac{\partial p_v}{\partial r} \right) + \frac{1}{r^2}\frac{\partial^2 p_v}{\partial \Theta^2} + \frac{\partial^2 p_v}{\partial z^2}. \end{aligned}$$

Here D is the diffusion coefficient of the condensing vapor within the carrier gas.

1.1 Simplifications

The partial time derivative of the temperature T and the partial vapor pressure p_v is zero, since the flow is in steady state. Moreover, the condenser is a circular tube, meaning that the profiles are axially symmetric, so all factors including Θ can be omitted. Since we assumed a laminar flow, also factors including v_r are zero. This leads to the following form of equations:

$$\begin{aligned} \frac{\rho C}{k} \cdot v_z \frac{\partial T}{\partial z} &= \frac{1}{r}\frac{\partial}{\partial r}\left(r\frac{\partial T}{\partial r}\right) + \frac{\partial^2 T}{\partial z^2}, \\ \frac{1}{D} \cdot v_z \frac{\partial p_v}{\partial z} &= \frac{1}{r}\frac{\partial}{\partial r}\left(r\frac{\partial p_v}{\partial r}\right) + \frac{\partial^2 p_v}{\partial z^2}. \end{aligned} \quad (3)$$

As mentioned before, we assumed a laminar flow, which means, that v_z can be replaced by a parabolic velocity profile:

$$v_z(r) = 2v_{mean} \cdot \left(1 - \frac{r^2}{R^2}\right). \quad (4)$$

Here v_{mean} is the average velocity in the z-direction and R is the inner diameter of the tube. The average velocity can be calculated from the volume flow rate in the tube:

$$v_{mean} = \frac{Q}{\pi R^2}. \quad (5)$$

1.2 Normalization

For the simulations, we normalized Equations (3, 4) with respect to R:

$$\begin{aligned} r' &= \frac{r}{R}, \\ z' &= \frac{z}{R}. \end{aligned} \quad (6)$$

Giving the following form of these Equations:

$$\begin{aligned} \frac{\rho C}{k} \cdot 2v_{mean} \cdot (1 - r'^2) \frac{\partial T}{\partial z' R} &= \frac{1}{r' R}\frac{\partial}{\partial r' R}\left(r' R\frac{\partial T}{\partial r' R}\right) + \frac{\partial^2 T}{\partial (z' R)^2}, \\ \frac{1}{D} \cdot 2v_{mean} \cdot (1 - r'^2) \frac{\partial p_v}{\partial z' R} &= \frac{1}{r' R}\frac{\partial}{\partial r' R}\left(r' R\frac{\partial p_v}{\partial r' R}\right) + \frac{\partial^2 p_v}{\partial (z' R)^2}. \end{aligned} \quad (7)$$

Simplifying:

$$\begin{aligned} \frac{\rho C}{k} \cdot R \cdot 2v_{mean} \cdot (1 - r'^2) \frac{\partial T}{\partial z'} &= \frac{1}{r'}\frac{\partial}{\partial r'}\left(r'\frac{\partial T}{\partial r'}\right) + \frac{\partial^2 T}{\partial z'^2}, \\ \frac{1}{D} \cdot R \cdot 2v_{mean} \cdot (1 - r'^2) \frac{\partial p_v}{\partial z'} &= \frac{1}{r'}\frac{\partial}{\partial r'}\left(r'\frac{\partial p_v}{\partial r'}\right) + \frac{\partial^2 p_v}{\partial z'^2}. \end{aligned} \quad (8)$$

For reasons of simplicity, we used the Peclet numbers for heat (Pe_T) and mass (Pe_{p_v}) diffusion:

$$\begin{aligned} Pe_T &= Re \cdot Pr = \frac{\rho \cdot v_{mean} \cdot 2R}{\mu} \cdot \frac{\mu \cdot C}{k}, \\ Pe_{p_v} &= Re \cdot Sc = \frac{\rho \cdot v_{mean} \cdot 2R}{\mu} \cdot \frac{\mu}{\rho \cdot D}. \end{aligned} \quad (9)$$

Here μ is the dynamic viscosity. This effectively results in the following form of the energy and the continuity equation:

$$\begin{aligned} Pe_T \cdot (1 - r'^2)\frac{\partial T}{\partial z'} &= \frac{1}{r'}\frac{\partial}{\partial r'}\left(r'\frac{\partial T}{\partial r'}\right) + \frac{\partial^2 T}{\partial z'^2}, \\ Pe_{p_v} \cdot (1 - r'^2)\frac{\partial p_v}{\partial z'} &= \frac{1}{r'}\frac{\partial}{\partial r'}\left(r'\frac{\partial p_v}{\partial r'}\right) + \frac{\partial^2 p_v}{\partial z'^2}. \end{aligned} \quad (10)$$

1.3 FEniCS Implementation

For the implementation in FEniCS, we needed to write the equations in variational form, which we achieved by multiplying with a test function u and integrating over the domain Ω:

$$\begin{aligned} -\int_\Omega \frac{1}{r'}\frac{\partial T}{\partial r'} \cdot u \, d\boldsymbol{x}' - \int_\Omega \left(\frac{\partial^2 T}{\partial r'^2} + \frac{\partial^2 T}{\partial z'^2}\right) \cdot u \, d\boldsymbol{x}' + Pe_T \cdot \int_\Omega (1 - r'^2)\frac{\partial T}{\partial z'} \cdot u \, d\boldsymbol{x}' &= 0, \\ -\int_\Omega \frac{1}{r'}\frac{\partial p_v}{\partial r'} \cdot u \, d\boldsymbol{x}' - \int_\Omega \left(\frac{\partial^2 p_v}{\partial r'^2} + \frac{\partial^2 p_v}{\partial z'^2}\right) \cdot u \, d\boldsymbol{x}' + Pe_{p_v} \cdot \int_\Omega (1 - r'^2)\frac{\partial p_v}{\partial z'} \cdot u \, d\boldsymbol{x}' &= 0. \end{aligned} \quad (11)$$

We used Green's formula to eliminate the second order derivatives in the first terms in both equations:

$$\begin{aligned} -\int_\Omega (\nabla^2 T) \cdot u \, d\boldsymbol{x}' &= \int_\Omega \nabla T \cdot \nabla u \, d\boldsymbol{x}' - \int_{\partial\Omega} \frac{\partial T}{\partial n} u \, ds, \\ -\int_\Omega (\nabla^2 p_v) \cdot u \, d\boldsymbol{x}' &= \int_\Omega \nabla p_v \cdot \nabla u \, d\boldsymbol{x}' - \int_{\partial\Omega} \frac{\partial p_v}{\partial n} u \, ds. \end{aligned} \quad (12)$$

Here $\partial\Omega$ denotes the boundary of the domain, on which the test function v is required to vanish, which means that the second terms on the right-hand side of equations (12) vanish ($\frac{\partial}{\partial n}$ is the derivative in the outward normal direction on the boundary). So, the energy and the continuity equation now have the following variational form:

$$\begin{aligned} -\int_\Omega \frac{1}{r'}\frac{\partial T}{\partial r'} \cdot u \, d\boldsymbol{x}' + \int_\Omega \nabla T \cdot \nabla u \, d\boldsymbol{x}' + Pe_T \cdot \int_\Omega (1 - r'^2)\frac{\partial T}{\partial z'} \cdot u \, d\boldsymbol{x}' &= 0, \\ -\int_\Omega \frac{1}{r'}\frac{\partial p_v}{\partial r'} \cdot u \, d\boldsymbol{x}' + \int_\Omega \nabla p_v \cdot \nabla u \, d\boldsymbol{x}' + Pe_{p_v} \cdot \int_\Omega (1 - r'^2)\frac{\partial p_v}{\partial z'} \cdot u \, d\boldsymbol{x}' &= 0. \end{aligned} \quad (13)$$

The simulation mesh goes from *r'=-1* to *r'=1* and from *z'=0* to *z'=Z/R*$_t$.

1.4 Saturation Profile

We simulated the temperature and the partial vapor pressures profiles separately. Subsequently, we calculated the Saturation profile, using the data of the simulations and the following relation for the saturation ratio S:

$$S = \frac{p_v}{p_{sat}}. \quad (14)$$

Here p_{sat} is the saturation vapor pressure, which we calculated from the temperature profile data (see next section).

1.5 Saturation Vapor Pressure

To calculate the saturation vapor pressure p_{sat} of the condensing vapor in air at the present temperature, we used the Antoine equation:

$$p_{sat} = 10^{A-\frac{B}{C+T}}. (15)$$

Here A, B and C are component specific constants.

2 Growth Model

The condensation particle growth model is based on Zhang and Liu (1990) and Sect. 13.4 of Hinds (1999). We calculated the growth model with the temperature, vapor pressure and saturation ratio profiles (Fig. 4) as input parameter. For Sup. Fig. S2 we evaluated the highest saturation ratio (which is at the centerline). The highest saturation ratio represents the smallest particle size that can be activated with this CPC. The smallest particles require the highest saturation ratio conditions to activate and grow, which is why we have chosen this case for Sup. Fig. S2. In both presented pressure cases (1000 hP and 250 hPa) the particles grow to sizes larger than 0.5 µm and can be considered as detectable (Zhang and Liu, 1990). Since the highest saturation ratio shifts towards the entrance of the condenser with lower pressure, the particles activate earlier and have more time to grow for lower pressure.

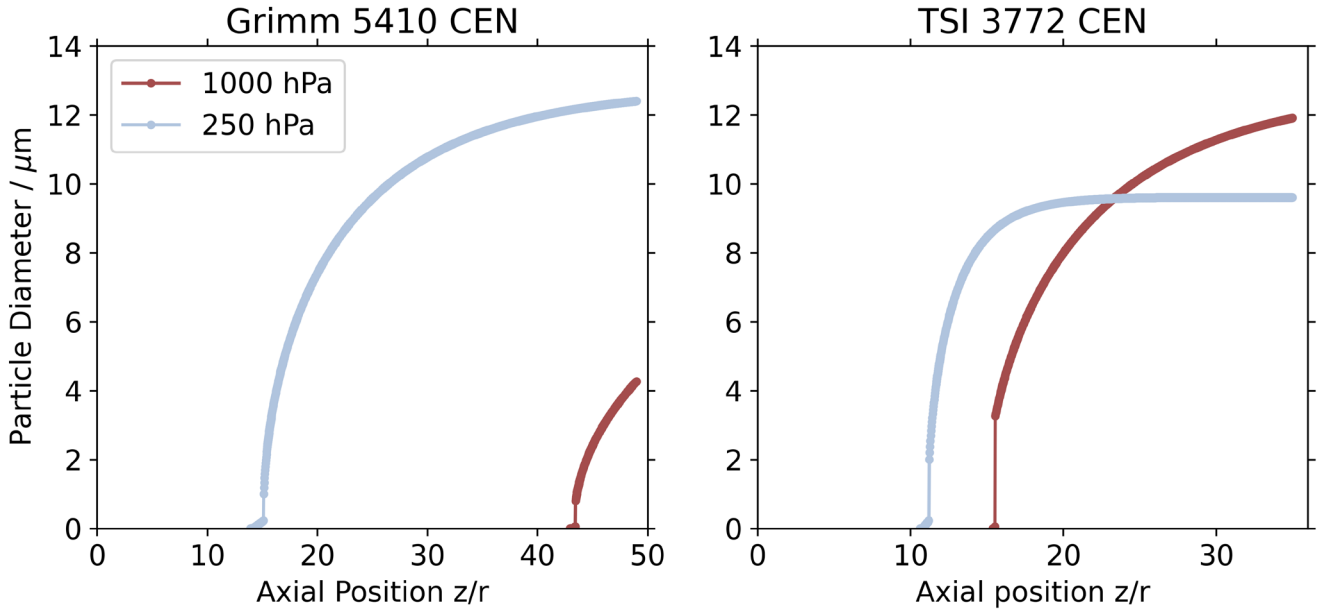

Figure S2: Example (left: Grimm 5410 CEN, right: TSI 3772-CEN) of the growth of the smallest particles that can be activated for 1000 hPa and 250 hPa. We calculated the growth model with the temperature, vapor pressure and saturation ratio profiles (Fig. 4 and Fig. 5) as input parameter.

3 Particle loss calculations

The particle loss calculation is based on parameters from ISO 15900:2009 (Kim et al., 2005; Wiedensohler et al., 2012): the dynamic gas viscosity, the mean free path and the Cunningham correction factor for different pressures and temperatures. The particle size-dependent diffusion coefficient was calculated with the Einstein- Sutherland-Smoluchowski relation, which is presented in many text books (Hinds, 1999; Seinfeld and Pandis, 2016; Kulkarni et al., 2011). For diffusional losses inside a normal tube we implemented Eq. (21) and Eq. (22) from Weiden et al. (2009). For the annular saturator in the Grimm CPC we used mainly Eq. (12) and Eq. (14) from Talebizadehsardari et al. (2020). The flow rates and temperatures for the each CPC are reported in Table 1 in the main manuscript.

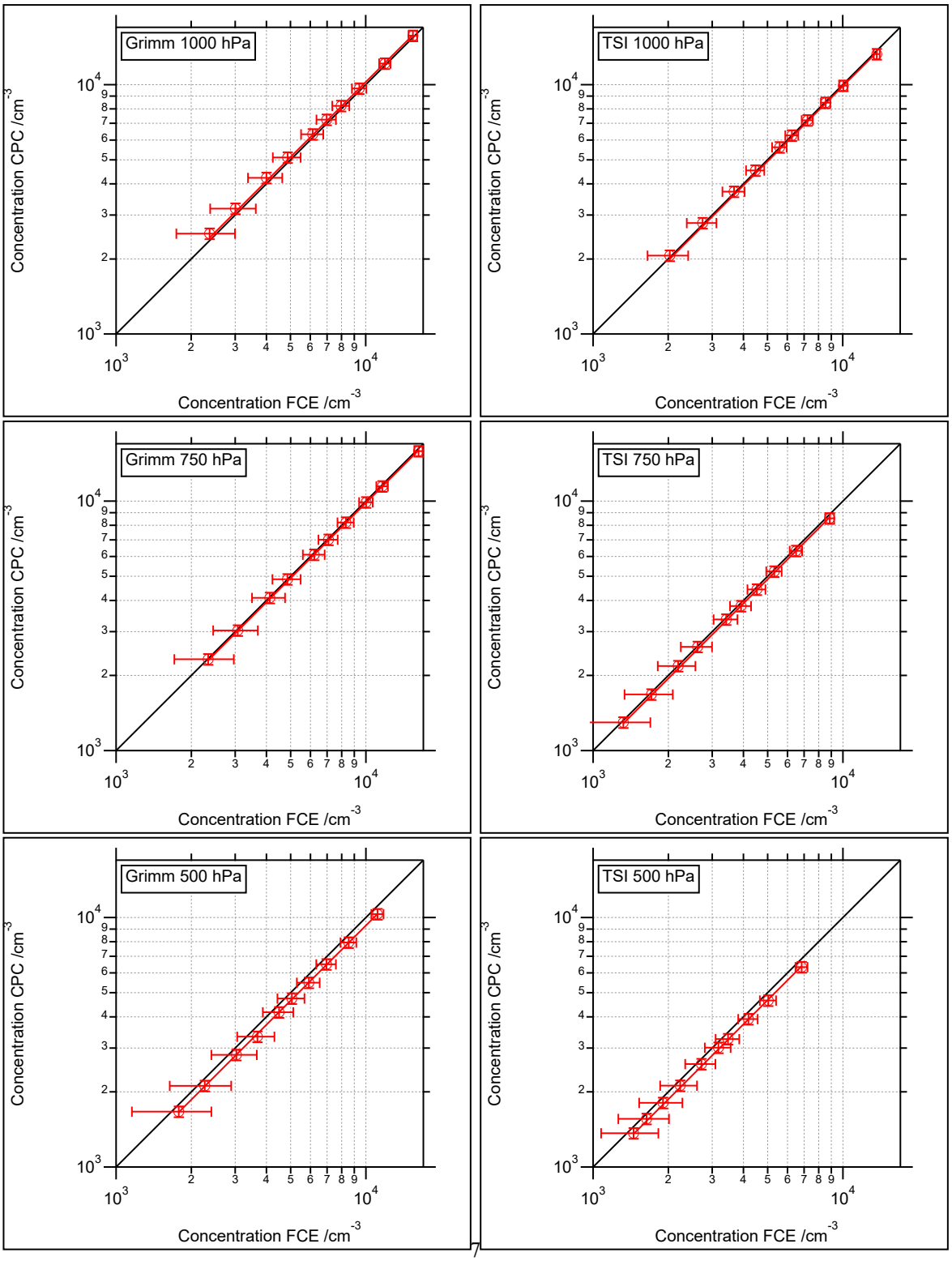
Grimm 1000 hPa
TSI 1000 hPa
Grimm 750 hPa
TSI 750 hPa
Grimm 500 hPa
TSI 500 hPa
Concentration CPC /cm-3
Concentration FCE /cm-3
10^3
10^4

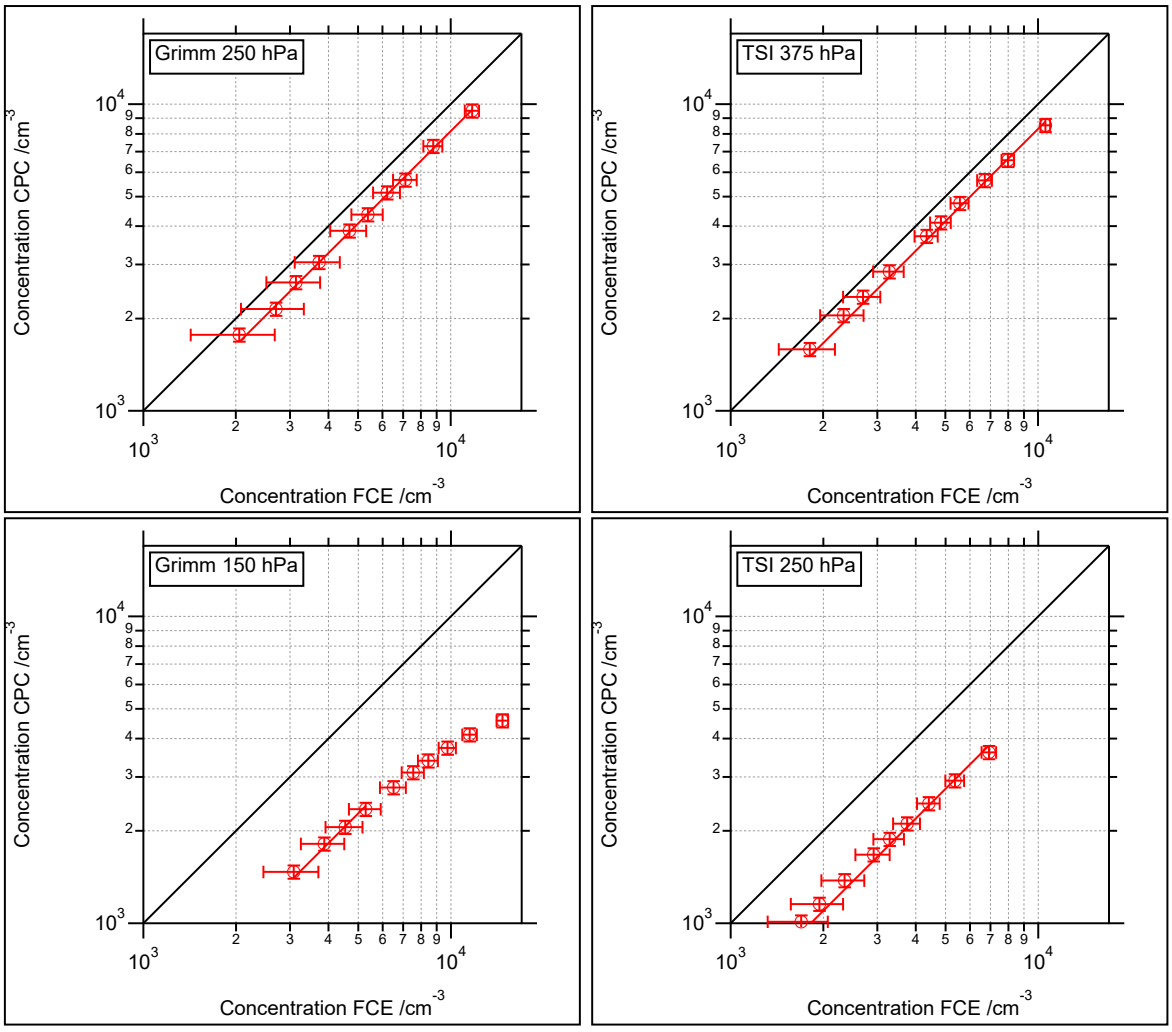

Figure S3: Linearity analysis of the CPC concentration (left: Grimm 5410 CEN, right: TSI 3772-CEN) compared to the FCE reference concentration for 30 nm particles. The black solid line represents the ideal 1:1 line. The red lines are linear fits through the origin (fit results with uncertainty in column CPC/FCE in Sup. Table S1). The Grimm CPC showed some non-linear response at 150 hPa and only data with FCE concentrations below 6000 cm^{-3} were considered for the linear fit.

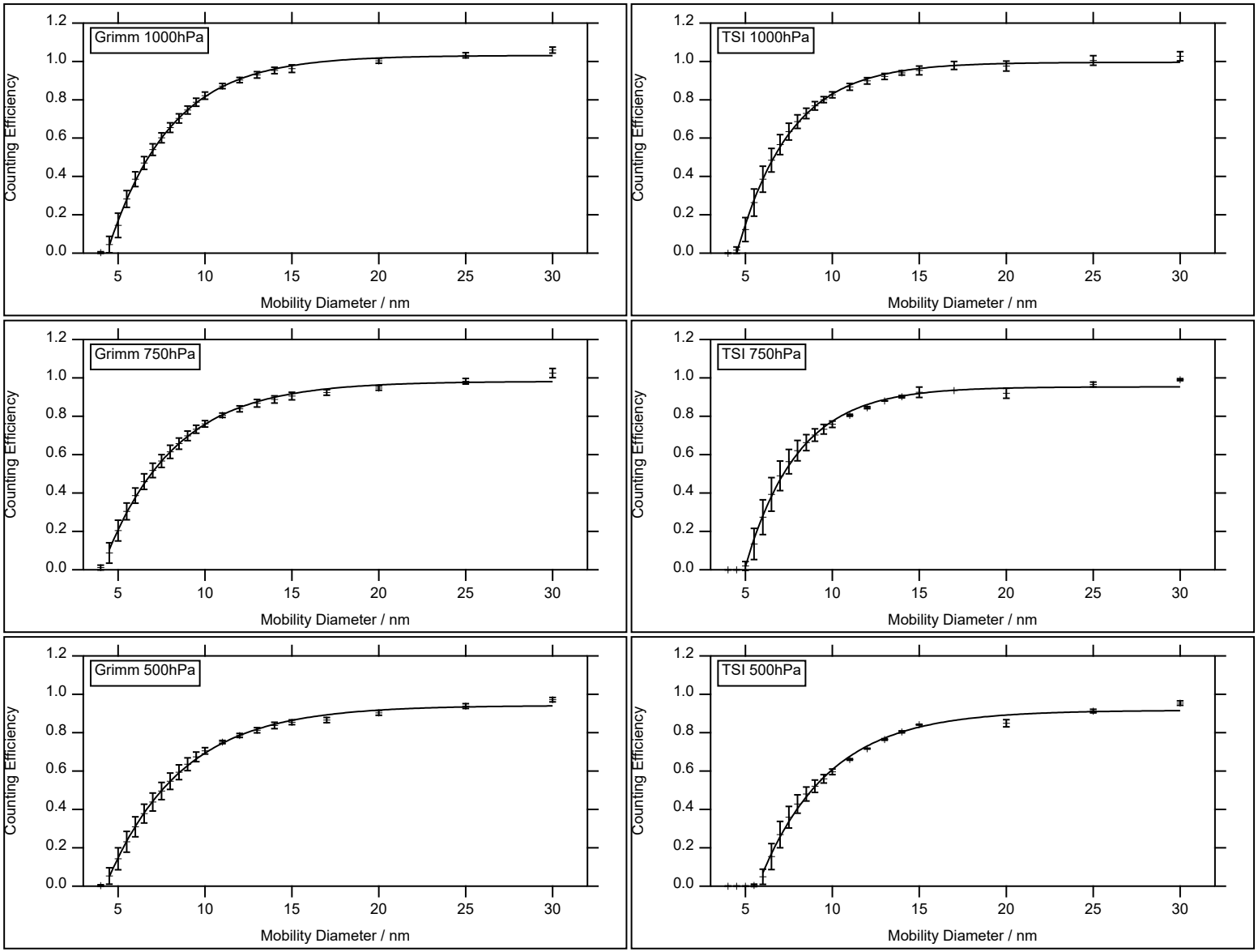
Grimm 1000hPa
TSI 1000hPa
Grimm 750hPa
TSI 750hPa
Grimm 500hPa
TSI 500hPa
Counting Efficiency
Mobility Diameter / nm
0.0
0.2
0.4
0.6
0.8
1.0
1.2
5
10
15
20
25
30

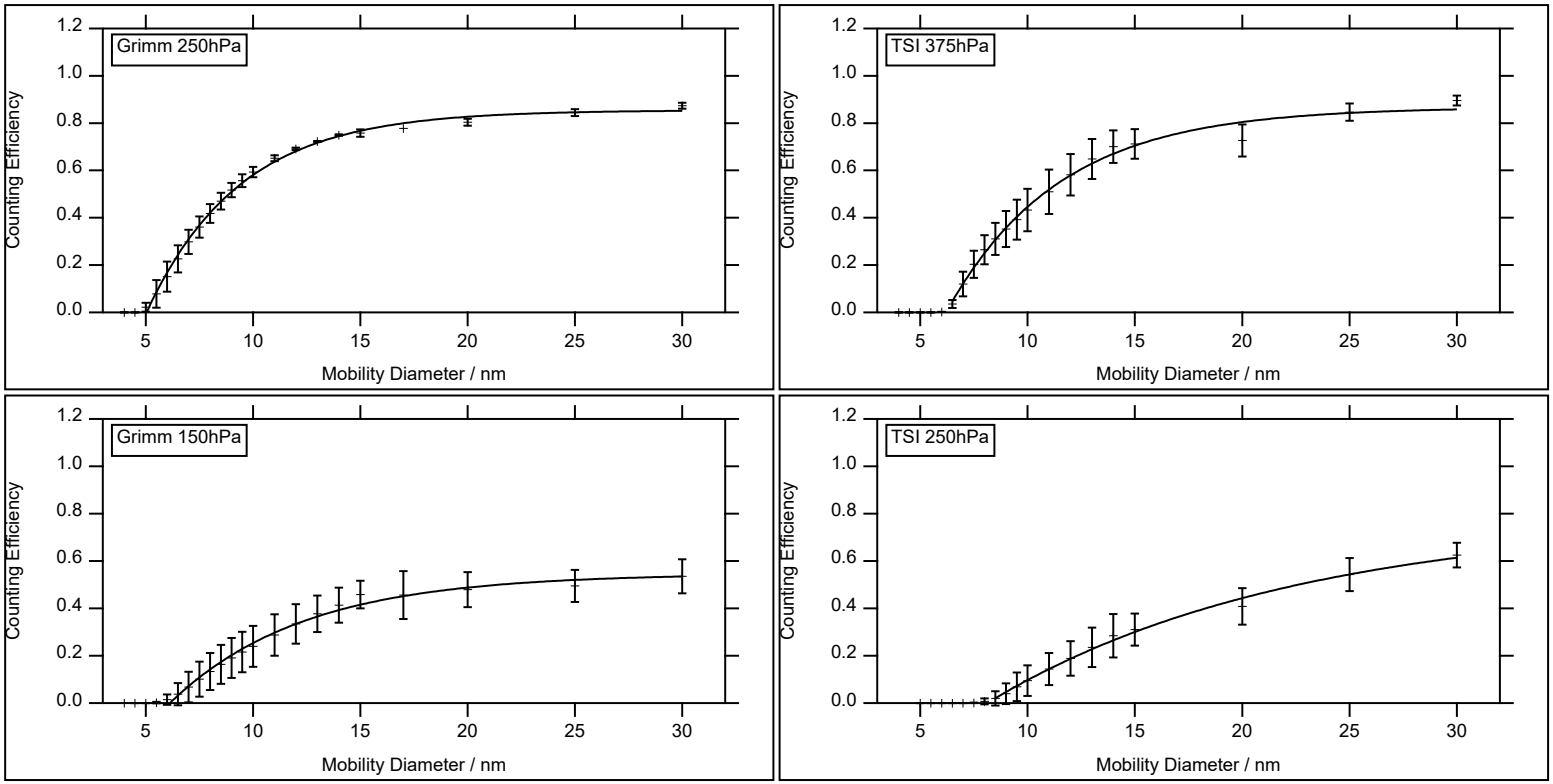

Figure S4: Counting efficiency curves (left: Grimm 5410 CEN, right: TSI 3772-CEN) as a function of the mobility diameter. The counting efficiency was measured with four Grimm CPCs and two TSI CPCs. The markers represent the average over the ensemble of each CPC-model. The error bars represent the standard deviation of the average. The fit is defined by the Eq. (3) and the parameters are reported with uncertainties in Sup. Table S1. The resolution of the DMA defined by the flow ratio was 1:10 for all measurements.

Table S1: Tab.2 of the main publication with the uncertainties of the fits. Results of the fits from Sup. Fig. S3 and Sup. Fig. S4 for the different CPC-models and pressure stages. The column CPC/FCE is the result of a linear fit through the origin of Sup. Fig. S3 comparing the concentration of the CPC to the FCE. The columns η_{plat}, $d_{p,0}$ and $d_{p,50fit}$ represent the fitting parameters of the counting efficiency Eq. (3) of Sup. Fig. S4.

CPC-model	Pressure [hPa]	CPC/FCE	η_{plat}	$d_{p,0}$ [nm]	$d_{p,50fit}$ [nm]
Grimm 5410 CEN	1000	1.0256 ± 0.0036	1.0313 ± 0.0061	4.36 ± 0.03	6.86 ± 0.04
Grimm 5410 CEN	750	0.9834 ± 0.0021	0.9817 ± 0.0075	4.05 ± 0.05	6.84 ± 0.05
Grimm 5410 CEN	500	0.9294 ± 0.0020	0.9416 ± 0.0067	4.27 ± 0.04	7.25 ± 0.05
Grimm 5410 CEN	250	0.8164 ± 0.0045	0.8546 ± 0.0089	5.04 ± 0.05	8.07 ± 0.08
Grimm 5410 CEN	150	0.4568 ± 0.0067	0.5463 ± 0.0146	6.13 ± 0.12	10.43 ± 0.25
TSI 3772-CEN	1000	0.9861 ± 0.0050	0.9954 ± 0.0061	4.50 ± 0.03	6.63 ± 0.04
TSI 3772-CEN	750	0.9730 ± 0.0030	0.9531 ± 0.0079	4.95 ± 0.04	7.04 ± 0.05
TSI 3772-CEN	500	0.9336 ± 0.0034	0.9165 ± 0.0128	5.69 ± 0.08	8.44 ± 0.10
TSI 3772-CEN	375	0.8308 ± 0.0073	0.8672 ± 0.0206	6.21 ± 0.13	9.85 ± 0.20
TSI 3772-CEN	250	0.5485 ± 0.0079	0.7808 ± 0.0495	8.12 ± 0.18	17.95 ± 1.06

References

Bird, R. B., Stewart, W. E., and Lightfoot, E. N.: Transport phenomena, J. Wiley, New York, 2002.

Hinds, W. C.: Aerosol Technology, Wiley-Blackwell, 1999.

Kim, J. H., Mulholland, G. W., Kukuck, S. R., and Pui, D. Y. H.: Slip Correction Measurements of Certified PSL Nanoparticles Using a Nanometer Differential Mobility Analyzer (Nano-DMA) for Knudsen Number From 0.5 to 83, 110, 31–54, https://doi.org/10.6028/jres.110.005, 2005.

Kulkarni, P., Baron, P. A., and Willeke, K. (Eds.): Aerosol Measurement, Third Edition., Wiley-Blackwell, 2011.

Seinfeld, J. H. and Pandis, S. N.: Atmospheric Chemistry and Physics, Wiley John + Sons, 2016.

Talebizadehsardari, P., Rahimzadeh, H., Ahmadi, G., Inthavong, K., Keshtkar, M. M., and Moghimi, M. A.: Nano-particle deposition in laminar annular pipe flows, 31, 3134–3143, https://doi.org/10.1016/j.apt.2020.06.005, 2020.

Weiden, S.-L. von der, Drewnick, F., and Borrmann, S.: Particle Loss Calculator – a new software tool for the assessment of the performance of aerosol inlet systems, 2, 479–494, https://doi.org/10.5194/amt-2-479-2009, 2009.

Wiedensohler, A., Birmili, W., Nowak, A., Sonntag, A., Weinhold, K., Merkel, M., Wehner, B., Tuch, T., Pfeifer, S., Fiebig, M., Fjäraa, A. M., Asmi, E., Sellegri, K., Depuy, R., Venzac, H., Villani, P., Laj, P., Aalto, P., Ogren, J. A., Swietlicki, E., Williams, P., Roldin, P., Quincey, P., Hüglin, C., Fierz-Schmidhauser, R., Gysel, M., Weingartner, E., Riccobono, F., Santos, S., Grüning, C., Faloon, K., Beddows, D., Harrison, R., Monahan, C., Jennings, S. G., O'Dowd, C. D., Marinoni, A., Horn, H.-G., Keck, L., Jiang, J., Scheckman, J., McMurry, P. H., Deng, Z., Zhao, C. S., Moerman, M., Henzing, B., Leeuw, G. de, Löschau, G., and Bastian, S.: Mobility particle size spectrometers: harmonization of technical standards and data structure to facilitate high quality long-term observations of atmospheric particle number size distributions, 5, 657–685, https://doi.org/10.5194/amt-5-657-2012, 2012.

Zhang, Z. Q. and Liu, B. Y. H.: Dependence of the Performance of TSI 3020 Condensation Nucleus Counter on Pressure, Flow Rate, and Temperature, 13, 493–504, https://doi.org/10.1080/02786829008959464, 1990.